The gyro-radius scaling of ion thermal transport from global numerical simulations of ion temperature gradient driven turbulence

M. Ottaviani[a)]
Département de Recherches sur la Fusion Contrôlée, Commissariat à l'Energie Atomique, Centre de Cadarache, 13108 St. Paul lez Durance, France

G. Manfredi[b)]
School of Cosmic Physics, Dublin Institute for Advanced Studies, Ireland

(Received 2 December 1998; accepted 27 April 1999)

A three-dimensional, fluid code is used to study the scaling of ion thermal transport caused by ion-temperature-gradient-driven (ITG) turbulence. The code includes toroidal effects and is capable of simulating the whole torus. It is found that both close to the ITG threshold and well above threshold, the thermal transport and the turbulence structures exhibit a gyro-Bohm scaling, at least for plasmas with moderate poloidal flow. © *1999 American Institute of Physics.* [S1070-664X(99)04908-3]

I. INTRODUCTION

In order to attain the ignition regime, it is crucial for a fusion device to display good confinement properties. Experimentally, the confinement time of toroidal fusion machines (tokamaks) has been growing steadily during the past decades. From the theoretical point of view, it is commonly accepted that confinement properties in the core of the tokamak are mainly determined by some form of low frequency (mainly electrostatic) turbulence, driven by the presence of equilibrium temperature and density gradients.

In the past few years, a subclass of gradient-driven turbulence, the ion-temperature-gradient (ITG) driven turbulence,[1,2] has received considerable attention by theoreticians. This is partly due to the fact that in large, neutral-beam heated tokamaks, the main thermal losses occur on the ion channel. There is, therefore, the hope that the study of a sufficiently accurate model of ITG turbulence would provide a rather good description of the ion losses in those regimes.

Our motivation for this work is somewhat more fundamental. We note that a suitably simplified model of ITG turbulence is a paradigm for many types of gradient-driven turbulence in toroidal geometry, and in particular gradient driven, small-scale, drift wave turbulence. Such a model should retain most of the qualitative feature of more accurate models. Thus one can hope that the study of the paradigm would produce information universal to the broader class to which the paradigm belongs. This approach is particularly useful when one is interested in the dependence of a given class of models on asymptotically small (or large) dimensionless control parameters, and the quantitative comparison with the amount of transport measured in a specific experiment is not an issue.

In this work we focus specifically on the problem of gyro-radius scaling of ion thermal transport, which is particularly crucial for the extrapolation of present experimental data to future larger devices. Our goal is to assess the dependence of ITG transport with the scale separation parameter $\rho_* = \rho_s / a$ where ρ_s is the ion sound Larmor radius (the Larmor radius measured at the electron temperature) and a is some macroscopic machine scale length (usually the tokamak minor radius). Note that the transport database studies carried out in the framework of the international thermonuclear experimental reactor (ITER) project[3] have demonstrated that a machine of the ITER type would perform better if the present data can be extrapolated according to the so-called gyro-Bohm scaling (see below).

Throughout this paper, ''large scale'' normalizations are adopted: Lengths are measured in units of a and times in units of $a^2/(cT_e/eB)$, where T_e is the electron temperature, B the toroidal magnetic field, e the electron charge, and c the speed of light. In these units, the transport coefficients are measured in Bohm units cT_e/eB. Thus, in general, the ion thermal conductivity χ will scale as $\chi \sim \rho_*^\alpha$, where $\alpha = 1$ for gyroradius scaling (the so-called gyro-Bohm scaling) and $\alpha = 0$ for Bohm scaling, and the dependence on other parameters like the temperature gradient, the safety factor, the magnetic shear, and the aspect ratio is not of primary concern in the present work.

Turbulent transport in tokamaks is given by small scale fluctuations of some typical length λ and time τ. At the machine scale $a \gg \lambda$, and for times of order of the energy confinement time $\tau_E \gg \tau$, it is usually assumed that transport can be mainly described as a diffusion-like process. It is natural to estimate the transport coefficients on the basis of simple dimensional arguments, based on the turbulence characteristic length and time, $\chi \sim \lambda^2/\tau$. The problem, of course, is that one does not know how to evaluate λ and τ. The estimates provided by linear theory are often unhelpful, since in many cases they have been shown to be inaccurate by direct numerical simulations and, indeed, there is no *a priori* reason why linear theory alone should be able to provide the

[a)]Electronic mail: mao@drfc.cad.cea.fr
[b)]Permanent address: Laboratoire de Physique des Milieux Ionisés, Université Henri Poincaré, Nancy-1, BP 239 F-54506 Vandoeuvre-les-Nancy cedex, France.

correct length and time scales for fully developed turbulence. The main (linear or nonlinear) ideas put forth to evaluate suitable λ and τ are briefly reviewed here.

In a cylinder, the radial extension of the linear eigenfunction scales as $\delta r_{\rm cyl} \sim \rho_*$. Therefore, identifying λ with $\delta r_{\rm cyl}$ and τ with the inverse of the mode frequency [which for ITG is the drift frequency $\omega_{*T}=(cT_e/eB)(k_\theta/L_T)$ associated with the temperature scale-length L_T], $\tau \sim \rho_*$, one could conclude that $\chi \sim \rho_*$ (gyro-Bohm scaling).

However, linear theory in a torus[4–6] shows that $\delta r_{\rm tor} \sim (\rho_s L_T)^{1/2} \sim \rho_*^{1/2}$ due to toroidal coupling, when the calculations are taken to second order[7] in the ballooning formalism.[8] Since the time scale is still given by the drift frequency, identifying λ with $\delta r_{\rm tor}$ leads to $\chi \sim$ const., independent of ρ_* (Bohm scaling).

In the nonlinear regime, analytical arguments[9] and numerical simulations have shown a tendency to isotropization in the poloidal plane, with radial and poloidal correlation lengths of similar size. A suitable λ would then be given by the inverse of a typical poloidal wave number, but this is difficult to evaluate. A plausible estimate could be given by the poloidal wave number of marginally stable modes. With this assumption, and replacing the parallel derivative operator with a constant, $\nabla_\parallel \to 1/(qR)$ (q is the safety factor and R the major radius), one obtains $\delta r \sim \rho_s (qR/L_T)$, which yields again a gyro-Bohm scaling.[10]

This latter argument, that linear structures are destroyed by the nonlinearities, seems plausible for strong input power, which brings the plasma well above the ITG marginal stability state. However, in the case of weak forcing, one can conjecture that the turbulence is not able to alter appreciably the form of the linear structures, which would then reach their saturation level essentially unchanged. (This occurs in several physical systems slightly above the instability threshold, for example in the case of Rayleigh–Benard convection, where the rolls, which are linear structures, survive unchanged in shape for not-too-strong temperature gradients.) If this were the case for ITG, it would open the possibility that, close to threshold, the transport scaling becomes of Bohm-type, due to the survival of the elongated linear structures.

In this work, we study the ρ_*-scaling of ion thermal transport in a torus, by means of direct numerical simulations of the ITG turbulence paradigm model, as described in the next section. In order to explore whether the nature of transport changes when one approaches the ITG threshold, the system is forced by various levels of input power; the corresponding turbulence ranges from near-threshold conditions to well-above-marginality conditions. The main conclusion is that, for all the cases so far studied, the ion thermal transport scales as gyro-Bohm. Some preliminary results from this study (for the case of forcing well above threshold) were presented in a previous paper.[11]

Several numerical investigations of this problem have recently appeared in the literature (for a partial review, see Ref. 12). Recently developed gyro-fluid codes are being used in flux-tube geometry—i.e., considering a small volume around a magnetic field line (local codes). Local codes generally assume *a priori* a gyro-Bohm scaling, and they are, therefore, not suited to address the ρ_*-scaling problem of ion transport.

On the other hand, particle-in-cell codes are used to solve the relevant gyro-kinetic equations in a finite region of the torus, much larger than the ion gyro-radius (global codes). Early results from global gyro-kinetic codes[13–15] pointed to a Bohm scaling for the ion thermal conductivity. The latest simulations by Lin *et al.*,[16] which include the self-consistent poloidal flows, did not address the gyro-radius dependence. However, the observable vortices appear to be smaller than in previous studies, thus suggesting the possibility that gyro-Bohm scaling could also occur in gyro-kinetic codes under certain conditions.

By comparison, our approach employs a fluid code in global geometry. We consider that a fluid model is adequate for our task, at this stage. Indeed, as previously discussed, much of the theoretical debate on the ρ_*-scaling has revolved around the generation and interaction of the turbulent structures in toroidal geometry. Thus, progress is made by understanding the role of the nonlinearities with respect to the linear turbulence drive and wave dispersion. Now, the relevant nonlinearities are fluid nonlinearities that can already be studied in a fluid context. Moreover, on the technical side, fluid models easily allow to study separately the role of the different terms entering in the equations, and the role of different approximations. In this respect they are a valuable complement to the analytic theoretical investigation. Of course a gyro-kinetic approach would give a more precise description of the plasma, and in particular would provide a more accurate determination of the instability threshold and of the Landau damping. However, a precise determination of the threshold does not seem to be required to study those aspects of the turbulent dynamics that are probably universal. We also stress the need to work in global geometry, since no *a priori* assumption is made on the size of the turbulent structures. Finally, note that with this choice at least two time scales come into play, the wave number-dependent turbulent time scale and the (global) transport time scale. In this respect, we opted to carry on most of the simulations until the system is stationary on the longest time scale—i.e., for at least one energy confinement time.

The fluid model utilized in this paper will be presented in Sec. II. In the spirit of working with a simplified model, and differently from the more detailed gyro-fluid models employed in local simulations, several parameters are only set to the correct order of magnitude, ignoring dimensionless factors which are presumably close to unity.

Section III will be devoted to a brief description of the numerical techniques. The numerical results will be presented in Sec. IV. Our conclusions are summarized in Sec. V.

II. THE PARADIGM FLUID MODEL FOR ITG TURBULENCE AND ION THERMAL TRANSPORT

A minimal (paradigm) model to describe ion thermal transport in a torus should include at least three evolution equations for the ion density, temperature, and parallel momentum. The electrons are assumed to be perfectly adiabatic,

and the quasi-neutrality equation provides the relationship between the ion density and the electrostatic potential that closes the system. The main toroidal term comes from the curvature drift in the continuity equation, and it is responsible both for driving the instability and for the coupling between neighboring poloidal modes, which is a specifically toroidal feature.

The paradigm ITG turbulence model employed in the present study is written as follows:

$$dw/dt + 2\epsilon\omega_d(\Phi + T_i) + A\nabla_\parallel v + (\kappa_n/r)\partial_\theta\Phi = D_w\nabla^2 w - \gamma_{\rm pfd}\rho_*^2\langle\Phi\rangle, \quad (1)$$

$$dv/dt + A\nabla_\parallel(\Phi + T_i) = D_v\nabla^2 v, \quad (2)$$

$$dT_i/dt + \Gamma\langle T_i\rangle A\nabla_\parallel v = -A\langle T_i\rangle^{1/2}|\nabla_\parallel| T_i + D_T\nabla^2 T_i, \quad (3)$$

where, $w=(\Phi-\langle\Phi\rangle)/T_e-\rho_*^2\nabla^2\Phi$ is the generalized vorticity (effectively the ion guiding center density), Φ is the electric potential, v the parallel ion velocity, T_i the ion temperature, $d/dt=\partial_t+\mathbf{v}_E\cdot\boldsymbol{\nabla}$ the advection operator, $\omega_d=(1/r)\cos\theta\partial_\theta+\sin\theta\partial_r$ the curvature operator, $\nabla_\parallel=(1/q)\times(q\partial_\phi+\partial_\theta)$ the parallel derivative operator, $\langle\bullet\rangle$ denotes flux surface average, $A=\epsilon/\rho_*$, and Γ is a constant. Units of T_e for the temperature, T_e/e for the potential and $c_s=(T_e/M_i)^{1/2}$ for the velocity are employed. The main control parameters are ρ_*, the aspect ratio $\epsilon=a/R$, and the equilibrium density gradient $\kappa_n=\nabla n_0/n_0$. Furthermore, D_w, D_v, and D_T are small artificial perpendicular dissipation coefficients set to damp the smallest scales and $\gamma_{\rm pfd}$ models the poloidal flow damping. The model is written for a low-β plasma with circular magnetic surfaces identified by the radial coordinate r; θ and ϕ are the poloidal and toroidal angles, respectively.

This model can be viewed as a simplified version of the ''3+1'' gyro-fluid model,[17] where the pressure tensor is taken to be isotropic and a number of finite Larmor radius (FLR) terms are dropped. This is justified by the interest in the dynamics of long wave lengths: If long wave lengths play a dominant role in determining the transport scaling, then FLR terms are irrelevant. Indeed, a shift of the peak of the spectrum from $\rho_s k_\theta\sim 1$ to larger scales is expected (and indeed observed) in the saturated nonlinear state.

The main damping mechanism is provided by parallel Landau damping, modeled by the $|\nabla_\parallel|$ term in Eq. (3), which stands for the operator whose representation in Fourier space is given by $|k_\parallel|$. This is the standard model of Landau damping employed in gyro-fluid codes.[18] With our normalization, the coefficient in front of this term must be of order unity, and in practice it is taken to be exactly one. Similarly, Γ is also set to unity, and the average ion temperature is taken to be equal to the electron temperature $\langle T_i\rangle=T_e=$ const. Thus Eqs. (1)–(3) must be reinterpreted as the equations of the evolution of difference between the ion temperature difference at a given point and the edge temperature, normalized to T_e/a.

Unlike the 3+1 gyro-fluid model, enforcing the isotropy of the pressure tensor prevents the model from effectively damping the self-generated poloidal flow. Therefore, the poloidal flow damping must be introduced artificially by setting $\gamma_{\rm pfd}$ with the correct scaling. Since the actual damping is proportional to the ion transit frequency $v_i/(qR)$,[17] one must take $\gamma_{\rm pfd}=\gamma_0(\epsilon/q\rho_*)$, where γ_0 is a constant of order one. It turns out that, with this choice of γ_0, the poloidal $\mathbf{E}\times\mathbf{B}$ flow is comparable to the diamagnetic flow. It was previously verified[17,19] that, when the flow damping is set to zero, the plasma accelerates and the transport drops substantially.

The domain of the simulation is a toroidal annulus between $r=r_a$ and $r=1$. We take $r_a=0.5$ throughout this study. All fluctuating components are set to zero at the boundaries. The macroscopic profiles (i.e., the $m=n=0$ components, where m and n are, respectively, the poloidal and toroidal wave numbers) of the vorticity w and the parallel velocity v are set to zero at $r=1$, while at $r=r_a$ their radial derivative is set to zero.

As to the electric potential Φ, the radial gradient of its $m=n=0$ component at the inner radius is an arbitrary parameter that we can freely adjust. This represents a radial electric field created in the inner region of the torus (between $r=0$ and $r=r_a$). Throughout this study, the radial derivative of the potential at r_a is taken to be zero.

The boundary condition for the ion temperature is more delicate. In order to achieve a stationary state, we want to inject energy in the system at a constant rate. This can be done by imposing the incoming flux of energy $F_{\rm in}=-D_T\nabla T_i$ at the inner radius r_a. In order to avoid excessively high gradients, it is convenient to set D_T relatively large at $r=r_a$, and then smoothly decrease it until it reaches its asymptotically small value at $r=r_b$. In the present study, $r_b=0.6$. We can then set the temperature gradient at r_a at a reasonable value—e.g., $\nabla T_i(r_a)=-1$, and adjust the thermal conductivity $D_T(r_a)$ in order to obtain the wanted value of the incoming flux $F_{\rm in}$. An increased D_T near the outer boundary was also employed in some of the runs (between $r=r_c=0.92$ and $r=1$), to reduce the build-up of a thermal boundary layer.

III. NUMERICAL METHOD

The system of equations [Eqs. (1)–(3)] is integrated numerically by means of a hybrid finite-difference-spectral method. The poloidal and toroidal angles are represented by their Fourier components, while finite differences are used for the radial variable. The nonlinear terms are computed in real space using a de-aliased fast fourier transform (FFT) algorithm, and then transforming back to Fourier space with an inverse FFT. Radial derivatives are computed using centered differences, thus the resulting code is second order accurate in space.

The time integration is more delicate, since different physical time scales are present in the model equations. In particular, the parallel and perpendicular time scales differ considerably in the interesting regime of small ρ_*. The perpendicular frequency is given essentially by $\omega_\perp=\omega_{T*}=\rho_s k_\perp(\rho_s/L_T)\Omega_i\simeq ak_\perp\rho_*^2\Omega_i$, assuming that $L_T\simeq a$ (Ω_i is the ion cyclotron frequency). The parallel time scale is given by ion sound waves with $\omega_\parallel=c_s k_\parallel=ak_\parallel\rho_*\Omega_i$. Their ratio is

$$\frac{\omega_\perp}{\omega_\parallel}=\rho_* \frac{k_\perp}{k_\parallel}. \tag{4}$$

For $k_\parallel \gtrsim k_\perp$ and small ρ_*, the parallel time scale is much faster than the perpendicular one. These short parallel wave lengths are not of physical interest, since they are rapidly removed by Landau damping. However, they impose a severe upper bound on the numerical time step ($\Delta t \omega_\parallel < 1$), if we work with an explicit time-advancing algorithm. It is therefore essential to employ an implicit scheme for the parallel dynamics, which lifts the above restriction and allows us to take $\Delta t \omega_\parallel > 1$. Although we do lose in accuracy when taking such large time steps, this is not dangerous insofar as small parallel wave lengths are strongly damped. The numerical scheme must, therefore, ensure that waves with large $k_\parallel$ are indeed damped for any value of the time-step. When this requirement is satisfied, there is no need to demand great numerical accuracy, since the physical model adopted to describe Landau damping is rather crude in the first place.

The interesting wave lengths are those for which $k_\parallel \lesssim \rho_* k_\perp$. In this case the parallel and perpendicular time scales are of the same order, and choosing $\Delta t \omega_\perp < 1$ gives sufficiently accurate results. For the perpendicular dynamics, we adopt an explicit scheme (second order leap-frog), for which the relation $\Delta t \omega_\perp < 1$ is sufficient to ensure stability.

A small amount of collisional dissipation is also introduced in our model, mainly for numerical reasons. This introduces a third time scale in our system $\omega_{diss} = D \rho_*^2 \Omega_i$ where D is the normalized viscosity (in Bohm units of $\rho_s^2 \Omega_i$). In order to avoid the possibility of numerical instabilities arising when the viscosity is large, we also use an implicit scheme for the collisional dissipation.

We have thus identified at least three different time scales in our system, corresponding to the parallel motion, perpendicular convection and collisional dissipation. Our strategy is to separate these three terms by means of a splitting technique, and then use different numerical schemes for each of them (explicit for the perpendicular dynamics, implicit for the other two terms). The splitting technique can be devised so as to guarantee second order accuracy in Δt for the resulting scheme. Our code is thus exact to second order both in space and in time.

The technique for time integration can be illustrated on a sample equation

$$\frac{dF}{dt}=(\hat{C}+\hat{P}+\hat{D})F. \tag{5}$$

The three operators $\hat{C}, \hat{P}$, and $\hat{D}$ denote, respectively, the nonlinear convective terms (including the curvature term ∂_Z), the parallel dynamics, and the dissipative terms. To second order in Δt, a formal solution of Eq. (5) from t_{n-1} to t_{n+1} is the following:

$$F_{n+1}=e^{\hat{P}\Delta t} e^{2\hat{D}\Delta t} e^{\hat{P}\Delta t} F_{n-1} + 2\Delta t e^{(\hat{P}+\hat{D})\Delta t} \hat{C} F_n. \tag{6}$$

F_{n+1} can thus be obtained in the following five steps:

(i) $F^*_{n-1}=e^{\hat{P}\Delta t} F_{n-1}$;
(ii) $F^{**}_{n-1}=e^{\hat{D}\Delta t} F^*_{n-1}$;
(iii) $F^*_{n+1}=F^{**}_{n-1}+2\Delta t \hat{C} F_n$;
(iv) $F^{**}_{n+1}=e^{\hat{D}\Delta t} F^*_{n+1}$;
(v) $F_{n+1}=e^{\hat{P}\Delta t} F^{**}_{n+1}$.

The convective operator $\hat{C}$ contains the nonlinear terms, and is thus treated explicitly with a leap-frog method (iii). The dissipation and parallel operators are linear, and the corresponding steps can be performed implicitly in order to guarantee numerical stability. For example, the dissipative dynamics [steps (ii) and (iv)] is solved with a Crank–Nicolson method, by approximating the exponential to second order

$$\exp(\hat{D}\Delta t)=\frac{1+\hat{D}\Delta t/2}{1-\hat{D}\Delta t/2}+O(\Delta t^3). \tag{7}$$

The parallel dynamics is treated in a similar way.

The code has been extensively tested in the linear regime (keeping the equilibrium profiles fixed), where direct comparison with theoretical results is possible for some simplified cases. Nonlinearly, the results have been qualitatively checked against results from gyro-kinetic codes, which describe a similar, albeit not identical, physics. Convergence of the results with respect to the resolution was verified routinely by inspection of the turbulent spectra, to check that negligible amount of energy resides at the grid boundary. In some cases, selected runs were carried out at incremented resolution for times comparable to the longest fluctuation time, for comparison. In practice, the resolution employed is comparable to the highest resolution reported in the gyro-kinetic literature.[16] In its present version, the code constitutes a reliable tool for the simulation of a nontrivial model of toroidal ITG turbulence.

IV. SCALING STUDIES IN THE NONLINEAR REGIME

In order to investigate the ρ_*-scaling problem, the code has been run with a nonzero energy flux $F_{\rm in}$ at the inner radius, until the system is in steady state. In principle this means that each simulation should be carried out for at least one energy confinement time. The actual duration of the simulation depends on the actual strength of the turbulence, which in turns is a function of the forcing parameter $F_{\rm in}$. In some cases, at higher resolution and when the confinement time is long, it was not feasible to go beyond one third or one half of a confinement time. We stress however that, because of the natural separation between the time and length scales of the turbulence and those of confinement, the duration of all the simulations is more than adequate, since the turbulence reaches a locally steady state in much shorter times.

In order to assess whether the transport exhibits a gyro-Bohm scaling, we proceed as it is usually done in similarity experiments. We start by carrying out a simulation at $\rho_* = \frac{1}{50}$ for a given input thermal flux $F_{\rm in}$, until the system reaches steady state. We then halve ρ_* to $\rho_* = \frac{1}{100}$ and at the same time we halve $F_{\rm in}$. If transport scales exactly like gyro-Bohm, that is, if the effective conductivity $\chi_{\rm eff}$ is proportional to ρ_* across the whole system

$$\chi_{\rm eff}=\rho_* f[r,\ \text{other parameters}\cdots], \tag{8}$$

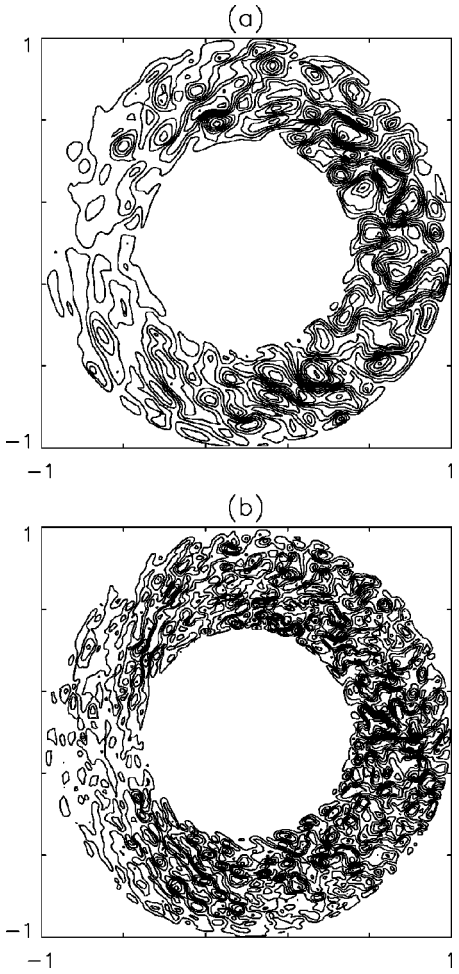

FIG. 1. Isolines of the electric potential for the cases (a), $\rho_*=\frac{1}{50}$, $F_{\rm in}=3\times10^{-2}$ and (b), $\rho_*=\frac{1}{100}$, $F_{\rm in}=1.5\times10^{-2}$.

then the two simulations should show the same profile. At the same time we can study how the turbulence changes with ρ_*, in particular by measuring the radial correlation length λ_c, the correlation time τ_c and the level of the fluctuations. A result of the form $\lambda_c\sim\rho_*$ would be consistent with the gyro-Bohm ideas.

With $\rho_*=\frac{1}{50}$ we use a resolution of $81\times128\times32$ (radial $\times$ poloidal $\times$ toroidal) points. Other parameters are $\epsilon=0.5$, $\gamma_0=0.25$, $D_w=D_v=D_T=1\times10^{-3}$. With $\rho_*=\frac{1}{100}$ the resolution is increased to $121\times192\times48$ and $D_w=D_v=D_T=5\times10^{-4}$.

In our series of studies at $\rho_*=\frac{1}{50}$, $F_{\rm in}$ ranges from $F_{\rm in}=1\times10^{-3}$, which leaves the system very close to threshold, up to $F_{\rm in}=3\times10^{-2}$, which brings the turbulence to a strong level.

The contour plot (isolines) of the fluctuating electric potential in a given poloidal plane (at a given toroidal location) are shown in Figs. 1(a) and 1(b), for the simulations at $\rho_*=\frac{1}{50}$, $F_{\rm in}=3\times10^{-2}$, and $\rho_*=\frac{1}{100}$, $F_{\rm in}=1.5\times10^{-2}$, respectively. This is the pair of cases farthest from threshold.

It is apparent that the size of the vortices depends strongly on ρ_*. In order to be more quantitative, we compute the normalized radial correlation function of the electric potential. For any given fluctuating quantity $\tilde{f}(r,\theta)$, defined on a given poloidal plane, we adopt the definition

$$C(\delta r)\equiv\langle\tilde{f}(r,\theta)\tilde{f}(r+\delta r,\theta)\rangle, \tag{9}$$

where the average is performed over r, θ, and a number of time slices (in statistically steady conditions). We can then proceed with the evaluation of the radial correlation length λ_c, defined as the width at half height of the correlation function—i.e., such that $C(\lambda_c)/C(0)\equiv\frac{1}{2}$. The result is $\lambda_c=0.050$ and $\lambda_c=0.026$ for $\rho_*=\frac{1}{50}$ and $\rho_*=\frac{1}{100}$, respectively, consistent with a gyro-Bohm scaling of ITG turbulence. The normalized radial correlation functions for these two cases are compared in Fig. 2, where the abscissa of the $\rho_*=\frac{1}{100}$ is stretched by a factor of 2, to make the ρ_* similarity explicit.

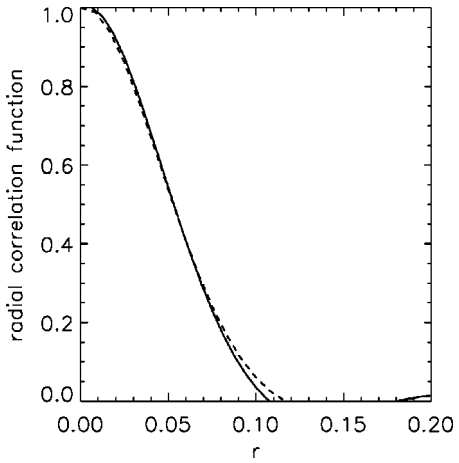

FIG. 2. Normalized radial correlation function for $\rho_*=\frac{1}{50}$, $F_{\rm in}=3\times10^{-2}$, solid line, and $\rho_*=\frac{1}{100}$, $F_{\rm in}=1.5\times10^{-2}$, dashed line. (The abscissa of the latter case is magnified by a factor of 2).

The ρ_* proportionality is also clearly exhibited by the correlation times. This is shown in Fig. 3 where the normalized time autocorrelation function [defined in the manner of Eq. (9)] is plotted against the normalized time difference $\delta t/\rho_*$.

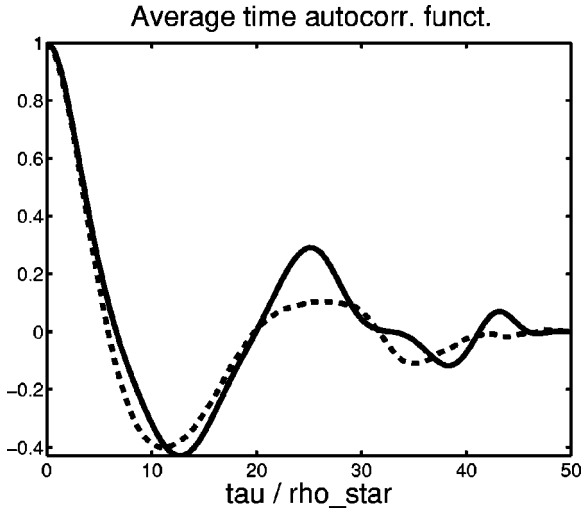

FIG. 3. Normalized time autocorrelation function for $\rho_*=\frac{1}{50}$, $F_{\rm in}=3\times10^{-2}$, solid line, and $\rho_*=\frac{1}{100}$, $F_{\rm in}=1.5\times10^{-2}$, dashed line. (The abscissa is normalized to ρ_*).

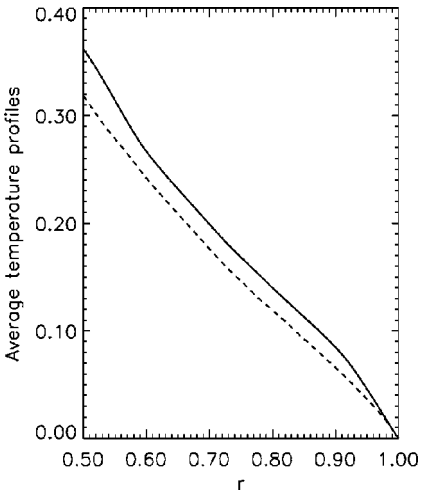

FIG. 4. Temperature profiles for $\rho_*=\frac{1}{50}$, $F_{\rm in}=3\times10^{-2}$, solid line, and $\rho_*=\frac{1}{100}$, $F_{\rm in}=1.5\times10^{-2}$, dashed line.

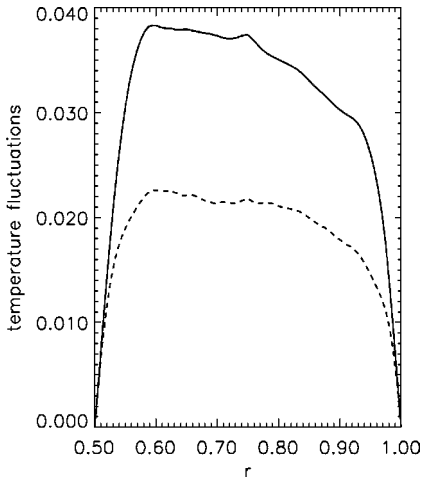

FIG. 6. Temperature fluctuations profile for $\rho_*=\frac{1}{50}$, $F_{\rm in}=3\times10^{-2}$, solid line, and $\rho_*=\frac{1}{100}$, $F_{\rm in}=1.5\times10^{-2}$, dashed line.

The crucial test of the similarity between the temperature profiles is shown in Fig. 4. One can see that the two profiles do not overlap as expected from an exact gyro-Bohm scaling. Quantitatively, the discrepancy is measured by the relative thermal energy, which is about 15%. Thus the effective conductivity in the whole domain of the numerical model, is not simply proportional to ρ_*.

A closer inspection reveals that the origin of the difference lies mainly in the behavior of the model in the buffer regions close to the boundaries. Here the turbulence decays from its nominal value far from the boundaries to zero at the boundaries. It turns out that this occurs over a length of the order of the turbulence correlation length, which itself scales like ρ_*. Thus the effective turbulent region is somewhat wider at smaller ρ_*, gradients are shallower in a wider region and, correspondingly, the overall transport somewhat larger. Strict similarity is broken since ρ_* does not only appear in the coefficient of Eq. (8), but also in its functional form, for values of the radial coordinate approaching the boundary. In order to show this, we plot the corresponding temperature gradients (Fig. 5). One can see that in the turbulent region—e.g., between $r=0.6$ and $r=0.9$, the gradients are essentially the same for the two cases, consistently with a gyro-Bohm scaling of the turbulent conductivity.

Further evidence supporting the gyro-Bohm scaling is provided by the temperature and potential fluctuations, averaged over the poloidal and toroidal angles and time. The profile of the temperature fluctuations is shown in Fig. 6. For a strict gyro-Bohm scaling, the fluctuations should scale as ρ_*. In the present case, a small correction to the exact gyro-Bohm scaling is observable also in the region where the turbulence is well developed—i.e., between $r\simeq0.6$ and $r\simeq0.9$ (besides the breakdown of strict similarity caused by the boundary regions as described above).

Finally, we define the effective turbulent thermal conductivity as

$$\chi_{\rm eff}=F/\nabla T_i=\langle v_{Er}T_i\rangle/\nabla T_i\,, \tag{10}$$

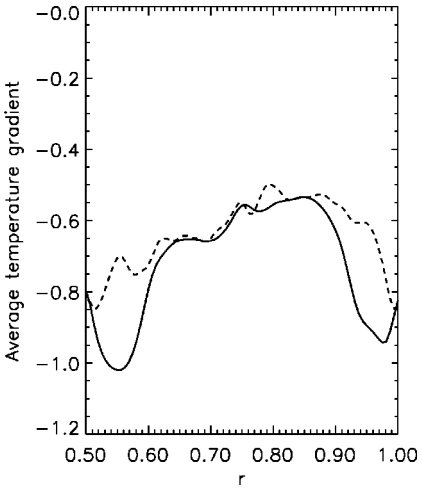

FIG. 5. Temperature gradients for $\rho_*=\frac{1}{50}$, $F_{\rm in}=3\times10^{-2}$, solid line, and $\rho_*=\frac{1}{100}$, $F_{\rm in}=1.5\times10^{-2}$, dashed line.

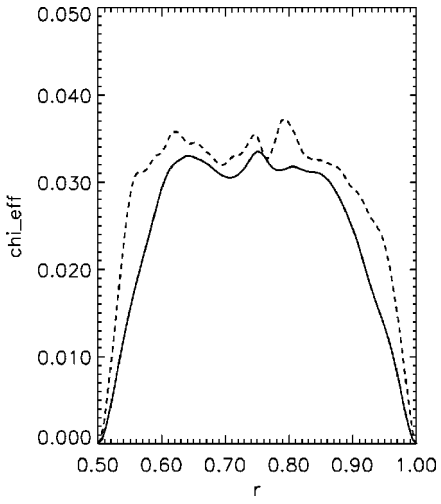

FIG. 7. Effective thermal conductivity for $\rho_*=\frac{1}{50}$, $F_{\rm in}=3\times10^{-2}$, solid line, and $\rho_*=\frac{1}{100}$, $F_{\rm in}=1.5\times10^{-2}$, dashed line. (The conductivity of the $\rho_*=\frac{1}{100}$ case is multiplied by a factor of 2.)

TABLE I. Correlation lengths.

F_{in}	ρ_*	λ_c
1.0×10^{-3}	0.02	0.035
5.0×10^{-4}	0.01	0.017
1.0×10^{-2}	0.02	0.047
5.0×10^{-3}	0.01	0.023
3.0×10^{-2}	0.02	0.050
1.5×10^{-3}	0.01	0.026

where the average is again over both angles and time. Figure 7 shows that χ_{eff} also scales almost as ρ_* in the turbulent region $0.6<r<0.9$. A possible reason for the observed correction to the exact gyro-Bohm scaling is discussed in the conclusions.

Similarity studies carried out at other values of the forcing gave similar results. The measured radial correlation lengths are summarized in Table I.

It is noteworthy that the gyro-Bohm scaling seems to hold even when the forcing is very weak and the system is very close to the ITG threshold. The contour plots for this case are shown in Fig. 8, and the corresponding profiles of the effective thermal conductivity in Fig. 9.

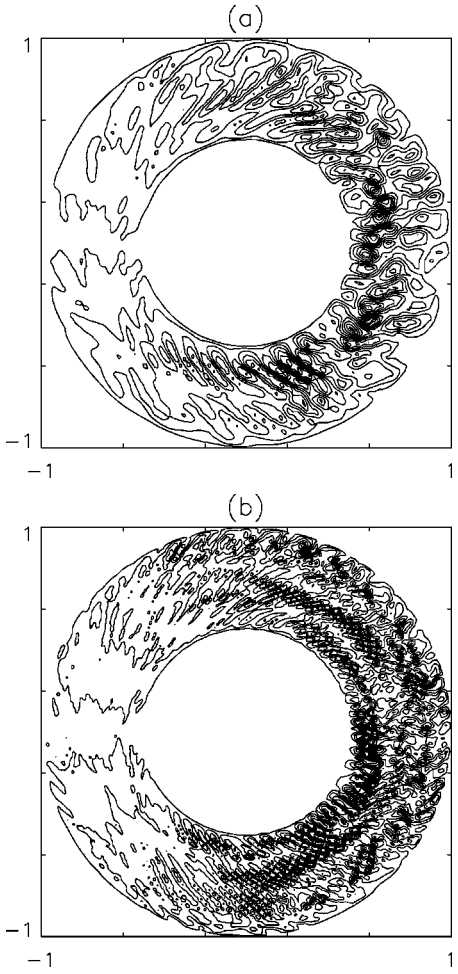

FIG. 8. Isolines of the electric potential for the cases (a), $\rho_*=\frac{1}{50}$, $F_{\text{in}}=1\times10^{-3}$ and (b), $\rho_*=\frac{1}{100}$, $F_{\text{in}}=5\times10^{-4}$.

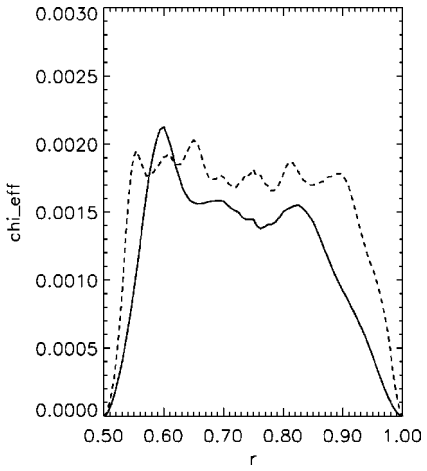

FIG. 9. Effective thermal conductivity for $\rho_*=\frac{1}{50}$, $F_{\text{in}}=1\times10^{-3}$, solid line, and $\rho_*=\frac{1}{100}$, $F_{\text{in}}=5\times10^{-4}$, dashed line.

Note that the results seem to validate the conjecture, advanced in the Introduction, that close to threshold the shape of the turbulent structures should resemble those given by linear theory. This is apparent from Fig. 8, where the field is predominantly composed by few high-m elongated objects. This should be confronted with the strong forcing case of Fig. 1, where the isotropic nonlinear interactions produce roundish vortices.

However, differently from what is usually found in linear theory, even close to threshold the size of the turbulent structures scales like ρ_* (Table I) and not like $\rho_*^{1/2}$. As a result, the ensuing transport still scales according to the gyro-Bohm law.

Finally, as a control case, we have performed a similarity experiment assuming that the scaling of thermal transport is purely Bohm. This can be done by keeping the incoming flux constant, while halving the value of ρ_*: If the transport were truly Bohm, then the effective thermal conductivity and the temperature gradient would remain the same. Therefore,

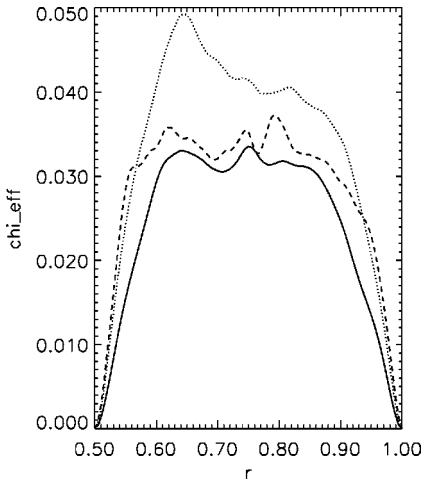

FIG. 10. Effective thermal conductivity for the control study: $\rho_*=\frac{1}{50}$, $F_{\text{in}}=3\times10^{-2}$, solid line, $\rho_*=\frac{1}{100}$, $F_{\text{in}}=1.5\times10^{-2}$, dashed line, and $\rho_*=\frac{1}{50}$, $F_{\text{in}}=1.5\times10^{-2}$, dotted line. (The conductivity of the last two cases is multiplied by a factor of 2.)

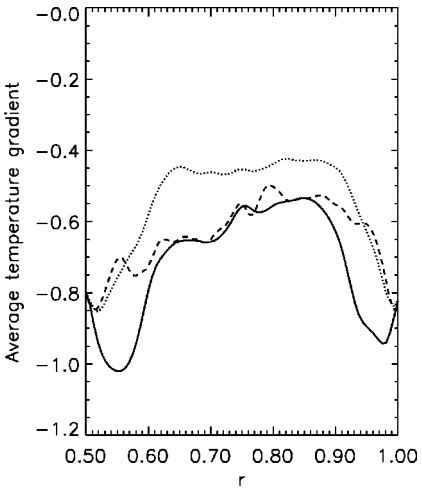

FIG. 11. Temperature gradients for the control study: $\rho_*=\frac{1}{50}$, $F_{\rm in}=3\times10^{-2}$, solid line, $\rho_*=\frac{1}{100}$, $F_{\rm in}=1.5\times10^{-2}$, dashed line, and $\rho_*=\frac{1}{50}$, $F_{\rm in}=1.5\times10^{-2}$, dotted line.

we compare the two cases $F_{\rm in}=1.5\times10^{-2}$, $\rho_*=\frac{1}{100}$, which is already available, and $F_{\rm in}=1.5\times10^{-2}$, $\rho_*=\frac{1}{50}$. The results are presented in Figs. 10 and 11, together with the reference case at $F_{\rm in}=3\times10^{-2}$ and $\rho_*=\frac{1}{50}$, and show that both the temperature gradient and the effective conductivity differ significantly in the two cases. From this control study, we can deduce that, for this model and in the present regime, the thermal transport is definitely closer to gyro-Bohm than to Bohm scaling.

V. CONCLUSION

In summary, we have found substantial numerical evidence that the paradigm fluid model for ITG turbulence in toroidal geometry exhibits a gyro-Bohm scaling, at least in all the cases studied, which are characterized by flat density profiles and weak poloidal rotation.

Whereas this result was expected in the regime of strong input power—i.e., well above the ITG threshold, as already found in a preliminary study,[11] the gyro-Bohm behavior near threshold is somewhat surprising. Indeed, although elongated structures similar to those given by linear toroidal theory were observed, as predicted, for near-threshold turbulence, those same structures still exhibit gyro-Bohm scaling. Thus our result invalidates our earlier speculations that the indication of Bohm behavior reported in some of the previous gyro-kinetic simulations[14,15] could be due to near threshold conditions.

Of course, if this difference were confirmed by longer global gyro-kinetic simulations (carried out with flux boundary conditions for a duration comparable to a confinement time), then this would be an indication that some important physics is not adequately described by the fluid models. In this respect, one should note that the contribution from the trapped ions is absent in our fluid model. The investigation of the role played by trapped ions on the scaling laws is an interesting subject for future gyro-kinetic simulations.

Note also that our result seem to support the procedure, normally used in local codes in flux-tube geometry, of simplifying the equations by neglecting higher order terms in asymptotically small values of ρ_*.

A sizeable deviation from a pure gyro-Bohm scaling can also be produced by a strong poloidal rotation.[20] The contribution from the rotation is second order in ρ_*, $\chi_{\rm eff}\sim\rho_*(1-\alpha\rho_*)$, with $\alpha\sim1$ for moderate rotation (like in the present simulations). It is interesting to note that this correction to a pure gyro-Bohm scaling would go in the direction shown in our simulations, that is it would cause a small increment (of a few percent) in the effective conductivity of the case $\rho_*=\frac{1}{100}$ with respect to what one would expect on the basis of a pure gyro-Bohm extrapolation from the corresponding $\rho_*=\frac{1}{50}$ case.

However, we have also noticed that a deviation from exact gyro-Bohm similarity of the numerically simulated profiles can be due to the boundary effect, since the boundary layer itself shrinks with ρ_* and the functional form of the total conductivity turns out to be ρ_*-dependent. This effect is the dominant one in our simulations which were carried out at moderate poloidal rotation. Specific studies with reduced poloidal damping, to make the rotation stronger, will be carried out to assess its effect on the turbulent transport.

Preliminary results with an equilibrium density gradient $\kappa_n\sim1$ show an increase in the radial jump of the electrostatic potential, so that the poloidal flow $v_\theta=-\partial_r\Phi$ and parallel flow also increase. A relatively steep density profile could therefore lead to a regime dominated by large bulk plasma flows and small transport coefficients. The presence of a superimposed radial electric field (also disregarded in the present simulations) could have a similar effect. The scaling of thermal transport in such regimes is still an open question which can be addressed in the future with the existing numerical code.

ACKNOWLEDGMENTS

The authors wish to thank M. Beer, X. Garbet, T. S. Hahm, and Z. Lin for a number of useful comments.

[1] W. Horton, D.-I. Choi, and W. M. Tang, Phys. Fluids **24**, 1077 (1981).
[2] B. Coppi and F. Pegoraro, Nucl. Fusion **17**, 5 (1977).
[3] ITER Confinement Database and Modelling Working Group (presented by G. Cordey), Plasma Phys. Controlled Fusion **39**, B115 (1997).
[4] J. W. Connor, J. B. Taylor, and H. R. Wilson, Phys. Rev. Lett. **70**, 1063 (1993).
[5] F. Romanelli and F. Zonca, Phys. Fluids B **5**, 4081 (1993).
[6] J. Y. Kim and M. Wakatani, Phys. Rev. Lett. **73**, 2200 (1994).
[7] D.-I. Choi and W. Horton, Phys. Fluids **23**, 356 (1980).
[8] J. W. Connor, R. J. Hastie, and J. B. Taylor, Proc. R. Soc. London, Ser. A **365**, 1 (1979).
[9] S. C. Cowley, R. M. Kulsrud, and R. Sudan, Phys. Fluids B **3**, 1803 (1991).
[10] M. Ottaviani, W. Horton, and M. Erba, Plasma Phys. Controlled Fusion **39**, 1461 (1997).
[11] G. Manfredi and M. Ottaviani, Phys. Rev. Lett. **79**, 4190 (1997).
[12] M. Ottaviani, M. A. Beer, S. C. Cowley, W. Horton, and J. A. Krommes, Phys. Rep. **283**, 121 (1997).
[13] H. E. Mynick and S. E. Parker, Phys. Plasmas **2**, 2231 (1995).
[14] Y. Kishimoto, T. Tajima, W. Horton, M. J. LeBrun, and J. Y. Kim, Phys. Plasmas **3**, 1289 (1996).
[15] R. D. Sydora, V. K. Decyk, and J. M. Dawson, Plasma Phys. Controlled Fusion **38**, A281 (1996).

[16]Z. Lin, T. S. Hahm, W. W. Lee, W. M. Tang, and R. B. White, Science **281**, 1835 (1998).
[17]M. A. Beer, *Gyro-fluid Models of Turbulent Transport in Tokamaks*, Ph.D. thesis, Princeton University (1995).
[18]G. W. Hammett and F. W. Perkins, Phys. Rev. Lett. **64**, 3019 (1990).
[19]G. Manfredi and M. Ottaviani, in *Theory of Fusion Plasmas*, edited by J. W. Connor, E. Sindoni, and J. Vaclavik (Editrice Compositori, Bologna, 1997), pp. 479–484.
[20]X. Garbet and R. Waltz, Phys. Plasmas **3**, 1898 (1996).